Bioorganic Chemistry 95 (2020) 103530

Contents lists available at ScienceDirect

Bioorganic Chemistry

journal homepage: www.elsevier.com/locate/bioorg

Design, synthesis and bioactivity evaluation of coumarin-chalcone hybrids as potential anticancer agents

Yu Wang[a], Wenda Zhang[b,*], Junqiang Dong[a], Jianbo Gao[a,*]

[a] Department of Radiology, The First Affiliated Hospital of Zhengzhou University, No. 1, East Jianshe Road, Zhengzhou 450052, Henan, China
[b] Department of Pharmacy, The First Affiliated Hospital of Zhengzhou University, No. 1, East Jianshe Road, Zhengzhou 450052, Henan, China

ARTICLE INFO

Keywords:
Thioredoxin reductases (TrxRs)
Xanthohumol (Xn)
Hybrids
Fluorescence
Mitochondrial apoptosis
Cancer therapy

ABSTRACT

The selenoprotein thioredoxin reductases (TrxRs) have been extensively studied as a potential target for the development of anticancer drugs. Herein, we designed, synthesized, and evaluated a series of coumarin-chalcone hybrids as TrxR inhibitors. Most of them exhibited enhancing anticancer activity than Xanthohumol (**Xn**). The representative **Xn-2** (IC_{50} = 3.6 μM) was a fluorescence agent, wherein drug uptake can be readily monitored in living cells by red fluorescence imaging. **Xn-2** down-regulated the expression of TrxR, remarkedly induced ROS accumulation to activate mitochondrial apoptosis pathway. Furthermore, **Xn-2** inhibited cancer cell metastasis and abolished the colony formation ability of cancer cells. Taken together, these results highlight that compound **Xn-2** may be a promising theranostic TrxR inhibitor for human cancer therapy.

1. Introduction

Thioredoxin reductase (TrxR) is the only known reductase to catalyze the reduction of oxidized Trx, the function of the thioredoxin system is strictly controlled by the activity of TrxR [1,2]. TrxR/Trx regulated the redox balance in many aggressive cancer cells, which is closely associated with many physiological processes of cancer cells such as proliferation, apoptosis, metastasis and angiogenesis [3–5]. The cellular ROS stress is regulated mainly by TrxR/Trx antioxidant systems under physiological conditions and caused by the decrease of mitochondrial membrane potential to induce apoptosis [6,7]. More importantly, mitochondria regulate the intrinsic apoptosis pathway that is governed by the proteins of the Bcl-2/Bax family [8]. Then, the activation of caspase cascades leads to cell death [9]. Therefore, owing to the essential and detrimental role of TrxR/Trx, the modulation of intrinsic apoptosis by TrxR inhibitors is a potential chemotherapeutic approach to eradicate cancer cells [10].

Structurally, all mammalian TrxR isomers are characterized by a penultimate selenocysteine residue (Sec498) at its conserved C-terminal (Gly-Cys-Sec-Gly) motif, which was the major target for TrxR inhibitors [11,12]. Accordingly, numerous TrxR-targeting compounds, especially, α, β-unsaturated ketones (such as chalcone and its derivatives) have been developed as potential irreversible TrxR inhibitors for anticancer treatment [13–15]. Natural products are the treasure for drug development, which have been providing novel skeletons and biological compounds to develop new drugs [16–21]. Nearly 60% drugs in the market are directly or indirectly derived from natural compounds [22]. Chalcones are privileged scaffolds in medicinal chemistry that possess a simple typical skeleton, bearing two phenyls (rings A and B) spaced by a *trans*-enone bridge [4]. Xanthohumol (Xn) is a structurally simple chalcone which is extracted from the hop plant, humulus lupulus. In addation, **Xn** has been widely used in some types of soft drinks, such as Julmust and Malta. What's more, Xn exhibits "broadspectrum" anticancer activity, and some putative anticancer mechanisms of **Xn** including generation of ROS, downregulation of anti-apoptotic proteins have been reported [11]. Despite the well-documented anticancer activity of Xanthohumol (**Xn**) is moderate, it is a good template compound as TrxR inhibitor to design more potent antitumor agents with special function for cancer therapy.

Natural and synthetical coumarin derivatives have multiple biological activities such as anticancer, anti-inflammatory, antioxidant and so on [23]. Moreover, a bulk of evidences showed that coumarin derivatives featured fluorescent characterization [24–26]. We hypothesized that new hybrids of 7-diethylamino-coumarin scaffold within chalcones might obtain novel fluorescent TrxR inhibitors. In this study, we discovered coumarin-chalcone hybrids as a new series of TrxR inhibitors with potent antitumor activity. These new inhibitors are promising candidates for further anticancer theranostic agents, due to their fluorescent properties and potent bioactivity.

* Corresponding authors.
E-mail addresses: zhangwenda16@126.com (W. Zhang), gaojianbo63@126.com (J. Gao).

https://doi.org/10.1016/j.bioorg.2019.103530
Received 10 September 2019; Received in revised form 25 November 2019; Accepted 19 December 2019
Available online 21 December 2019

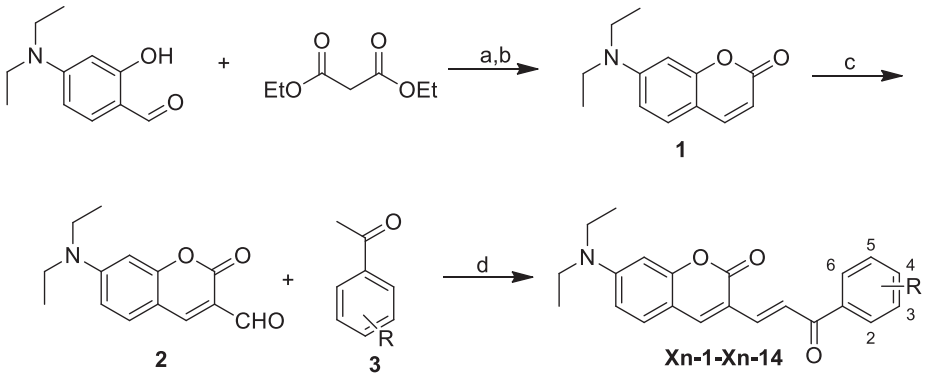

Scheme 1. Synthesis of (E)-7-(diethylamino)-3-(3-oxo-3-phenylprop-1-en-1-yl)-2H-chromn-2-ones. a, Piperidine, EtOH; b, HOAc, HCl; c, POCl 3 , DMF; d, Piperidine, HOAc, n-butyl alcohol.

2. Results and discussion

2.1. Synthesis of coumarin-chalcone hybrids

A solution of 4-(diethylamino)-2-hydroxybenzaldehyde and diethyl malonate in ethanol with piperidine obtained the crude ethyl 7-(diethylamino)-2-oxo-2H-chromene-3-carboxylate (**1**). The crude compound **1** was dissolved in hydrochloric acid and glacial acetic acid to obtain the pure 7-(diethylamino)-2H-chromen-2-one (**2**). Dry DMF was added dropwise to $POCl_3$ and 7-(diethylamino)-2H-chromen-2-one was added to obtain 7-(diethylamino)-2-oxo-2H-chromene-3-c-arbaldeh-yde (**3**). The desired compound **Xn-1**-**Xn-14** were accomplished by reaction compound 3 with acetophenones (Schemes 1 and 2). All of the coumarin-chalcone hybrids were confirmed by ^{1}H NMR, IR, HRMS (ESI) spectra, and ^{13}C NMR spectrum. The respective ^{1}H NMR, ^{13}C NMR, HRMS (ESI) and IR spectrums of **Xn-2** (Figure S1-4).

2.2. Biological evaluation

2.2.1. In vitro cell growth inhibitory activity

To summarize the structure-activity relationships of the synthetic compounds, colon carcinoma HCT116 cells were treated with designed compounds and the positive control, **2** and **Xn**, by MTT assay. The IC_{50} values were summarized in Table 1. Notably, most of the compounds exhibited better activity than **Xn** and **2**. It was obvious that the substitutes in bezene ring of the derivatives significantly affected their antitumor activity. Generally, the activity of 3-OH derivatives (such as **Xn-2, Xn-18**) exhibited better activity. Additionally, the activity of halogen-substituted derivatives (such as **Xn-8, Xn-11**) exhibited moderate activity except 4-F derivative **Xn-7** with IC_{50} values of 3.91 μM. 4-NH_2 derivative **Xn-14 (**$IC_{50,}$ 10.22 μM**)** exerted more potent than that of

Table 1
Anti-proliferative activity of the designed compounds and reference **Xn**.

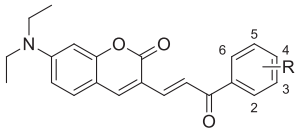

Compd	R	HCT116
		IC_{50} ± SD (μM)[a]
Xn-1	3,4-$(OCH_3)_2$	14.90 ± 0.28
Xn-2	3-OH-4-OCH_3	3.60 ± 0.06
Xn-3	3-OCH_3	17.10 ± 0.29
Xn-4	4-CH_3	18.89 ± 0.51
Xn-5	2-CH_3	16.30 ± 3.01
Xn-6	3-CH_3	22.09 ± 1.32
Xn-7	4-F	3.91 ± 0.37
Xn-8	4-Br	19.42 ± 0.28
Xn-9	4-C_4H_9	22.81 ± 1.15
Xn-10	4-OC_2H_5	19.80 ± 1.31
Xn-11	2,4-Cl_2	24.4 ± 1.62
Xn-12	3-OH	9.98 ± 0.14
Xn-13	4-NO_2	19.70 ± 0.54
Xn-14	4-NH_2	10.22 ± 0.14
2	–	> 100
Xn	–	27.60 ± 1.50

The inhibitory effects of the compounds on the proliferation of HCT116 cell line were determined by the MTT assay for 72 h. SD: standard deviation, all experiments were independently performed at least three times.

4-NO_2 derivative **(**$IC_{50,}$ 19.70 μM**).** Among them, the most potent compound **Xn-2** inhibited the growth of HCT116 cells with IC_{50} values of 3.60 μM, which had ~ 8 fold improvement in antitumor activity than

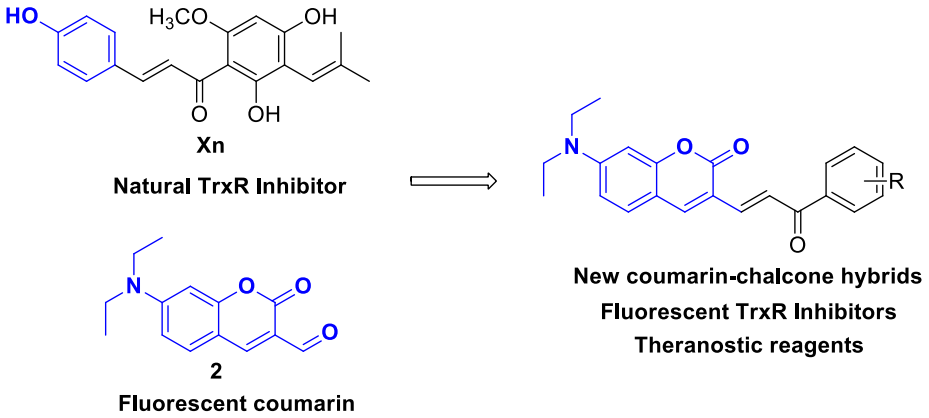

Scheme 2. The design of courmarin-chalcone hybrids as new TrxR inhibitors.

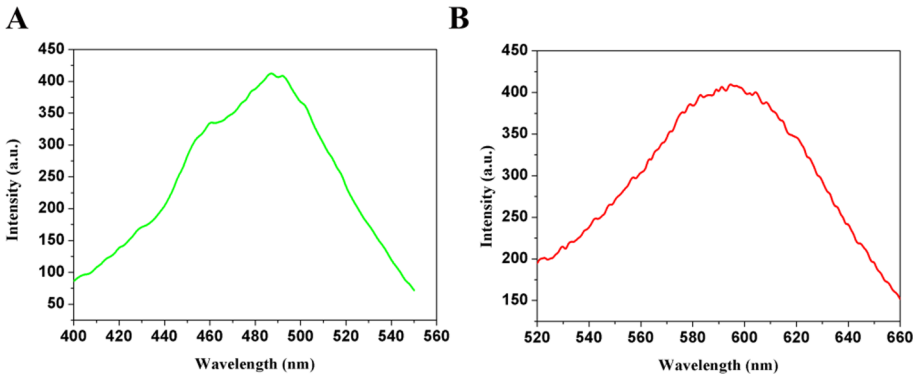

Fig. 1. Excitation and emission spectra of **Xn-2** at 10 μM in PBS solution.

Xn and more potent activity than its individual moiety **2** (IC_{50} > 100 μM).

Next, the fluorescent characterization of **Xn-2** was investigated to confirm its bio-monitoring application. As shown in Fig. 1, the fluorescent properties of **Xn-2** showed that the maximum excitation and emission peak are at 490 nm and 595 nm, respectively. **Xn-2** featured a large Stokes Shift (105 nm) which was suitable for bioimaging [27,28]. Considering the excellent sensing properties of the probe in vitro system, we further explored its capability of bioimaging by cell uptake assay in cancer cells. As shown in Fig. 2, the cells treated with **Xn-2** exhibited enhancing fluorescence response signal in a dose-dependent manner. These results indicated that **Xn-2** possessed obvious advantage and high practical value for biological imaging.

To confirm **Xn-2** as a TrxR inhibitor, the effect of **Xn-2** on TrxR was investigated by western blot analysis. HCT116 cells were incubated with **Xn-2** and the levels of TrxR were then examined. **Xn-2** suppressed the levels of TrxR protein in a concentration-dependent manner (Fig. 3). Thus, these data suggested that **Xn-2** was a potent TrxR inhibitor. The TrxR system is crucial for the intracellular redox balance to prevent excess ROS accumulation in mitochondria. Inhibition of TrxR may disturb the redox balance, leading to intracellular ROS accumulation in cancer cells. Accordingly, we examined the impact of **Xn-2** on ROS levels in HCT116 cells. Cells were treated with various concentrations of **Xn-2**. The levels of intracellular ROS were determined by measuring the fluorescent signals using ImageXpress Micro Confocal analysis. As shown in Fig. 4, treatment with **Xn-2** rapidly and significantly increased the levels of intracellular ROS, which was partially abrogated by pretreatment with 10 mM *N*-acetyl-L-cysteine (NAC). These data indicated that **Xn-2** was a potent TrxR inhibitor and promoted ROS accumulation in colon cancer cells.

Mitochondria, as the most important organelle, play a great role not only in supplying metabolic energy to the cell, but also in regulating the signal transmission during the apoptosis of cancers. Besides, although electron transport chain in mitochondria is the vital resource of intracellular ROS, the mitochondrial dysfunction can be aroused under the high ROS exposure. Mitochondria dysfunction causes up-regulation

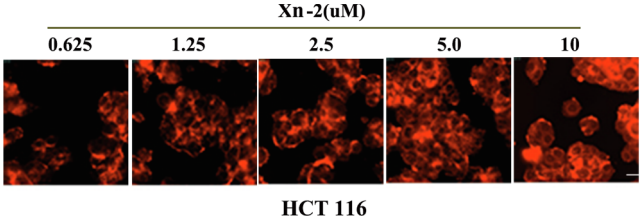

Fig. 2. Fluorescence imaging of **Xn-2** in HCT116 cells using different concentrations. Fluorescence images of HCT116 cells treated with **Xn-2** at concentration of 0.625, 1.25, 2.5, 5.0, and 10 μM for 1 h. The images were captured and imaged using an ImageXpress Micro Confocal analysis. Scale bar: 20 μm.

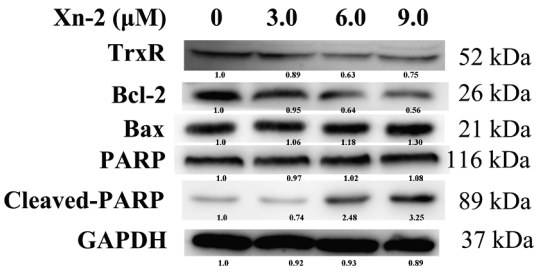

Fig. 3. Effects of **Xn-2** on the expression levels of TrxR, Bcl-2, Bax, Cyt c, PARP and Cleaved-PARP. Western blot analysis of TrxR, Bcl-2, Bax, PARP and Cleaved-PARP levels in whole-cell lysates of equal total protein prepared from HCT116 cells treated with compound **Xn-2** for 24 h. The images were captured and analyzed by Image Lab 3.0 software.

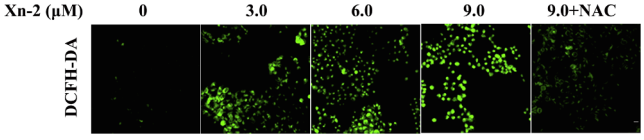

Fig. 4. Induction of ROS accumulation by **Xn-2**. HCT116 cells were stained with DCFH-DA after treatment with **Xn-2** or NAC (10 mM). Scale bar: 20 μm.

the ratio of apoptosis protein Bax/Bcl-2 and spurs Cyt c secretion to cytoplasm which induces the apoptosis of cancer cells. We further investigated the effect of **Xn-2** on the expression of Bcl-2, Bax and cleaved-PARP. As shown in Fig. 3, the expression level of Bcl-2 was decreased and the level of Bax was up-regulated with the increasing concentration of **Xn-2**, which activated the mitochondria caspase cascades and induced the cleavage of PARP (Fig. 3).

The aforementioned has elucidated that **Xn-2** inhibited TrxR to activate the mitochondria-mediated apoptosis cascades. Subsequently, we investigated the apoptosis of HCT116 cells induced by **Xn-2.** Cells were treated with **Xn-2** and stained by Hoechst 33342. As Fig. 5 showed, an increasing number of cells displayed condensed nuclei, a

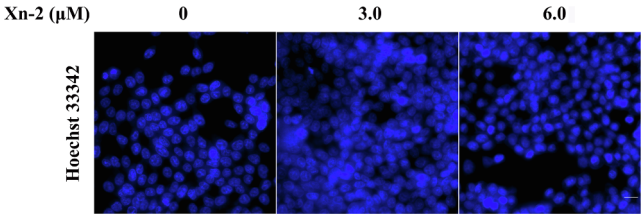

Fig. 5. Xn-2 induced Nuclear shrinkage to induce apoptosis. HCT116 cells were stained with Hoechest 33342 after treatment with **Xn-2** for 24 h. The images were captured and imaged using an ImageXpress Micro Confocal analysis. Scale bar: 20 μm.

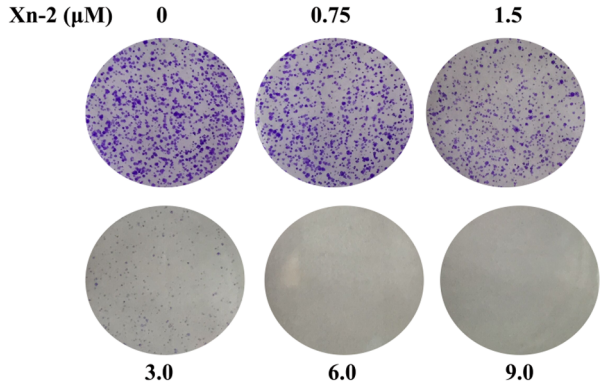

Fig. 6. Compound **Xn-2** inhibited the colony formation of HCT116 carcinoma cells. HCT116 cells were treated with compound **Xn-2** at 0.75–9.0 μM for 24 h and cultured for 14 d until the colonies were visible. Crystal violet solution was used to stain the colonies for 4 h and imaged.

characteristic morphology of cells undergoing apoptosis.

To further investigate the anti-proliferative activity of compound **Xn-2** on cancer cells, colony survival assay was performed. HCT116 cells were treated with compound **Xn-2** at 0.75–9.0 μM for 24 h and cultured for 14 d until the colonies were visible. Crystal violet solution (Sigma, St. Louis, MO, USA) was used to stain the colonies for 4 h and imaged. As shown in Fig. 6, a significant reduction in clonogenic ability at 1.5 μM of compound **Xn-2** and an almost cessation of colony formation at 6 μM.

Metastasis is directly or indirectly responsible for the majority of cancer deaths. Anti-metastasis treatment is thus the key to cure cancer. To investigate the inhibitory effect of **Xn-2** on tumor migration, a *trans*-well assay was performed. In the presence of **Xn-2** at 3.0 μM, the migration of HCT116 cells was effectively suppressed (Fig. 7), revealing that **Xn-2** was a new anti-metastasis agent.

The mechanism of inhibition of TrxR may be derived from its alfa, beta-unsaturated ketone structure, which modify the highly reactive selenocysteine residue of TrxR to inhibit the enzyme activity [29–32]. Furthermore, the potential binding mode of Xn with TrxR protein was predicted by docking experiments. As Fig. 8 shown, Xn could bind tightly to TrxR by forming four hydrogen bonding interactions with the Cys497, Val484 and Ser404 residues in the C-terminal active site. In addition, the residue Sec498 swings around the alfa, beta-unsaturated ketone of Xn, which may form an irreversible binding. Taken together, all this may provide a rationale explaining the interaction of Xn with TrxR.

3. Conclusions

New theranostic probe, coumarin-chalcone hybrid Xn-2 with red fluorescence has been developed as antitumor agent. Studies showed that Xn-2 could be efficiently delivered to cells to induce apoptosis. The probe accumulated in cancer cells efficiently spurred the generation of

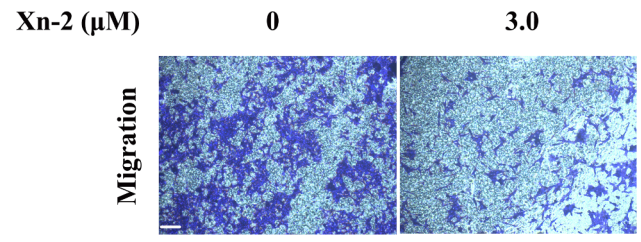

Fig. 7. The effect of **Xn-2** on tumor metastasis by *trans*-well migration assay. HCT116 cells and **Xn-2**-treaed HCT116 cells were seeded in a transwell chamber and incubation for 24 h, then fixed by 4% paraformaldehyde, and dyed by crystal violet and imaged under microscope. Scale bar: 50 μm.

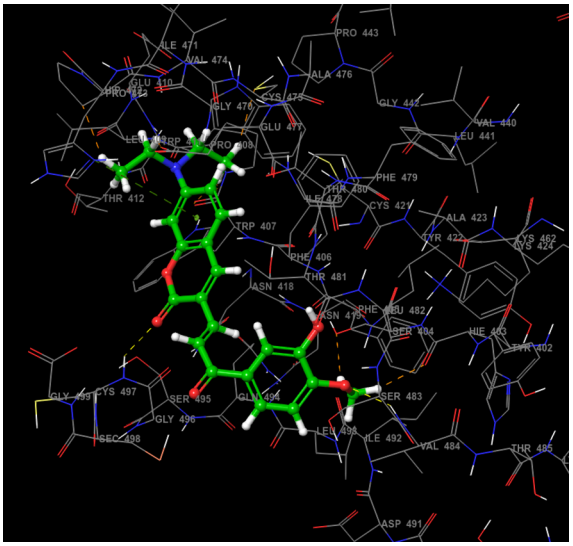

Fig. 8. Molecular docking of Xn at the C-terminal active site of rat TrxR using Maestro 9.4. Hydrogen bonds were shown as dashed lines.

intracellular ROS, then triggered cancer-cell apoptosis. This strategy of combing a small-molecule fluorescent dye within a natural active compound may represent a versatile method for the design of theranostic probes. There are some TrxR probes, which mainly contain α, β-unsaturated ketones or an activable disulfide bond [33,34]. Interestingly, Xn also has α, β-unsaturated ketone with red emission and may not only be used as a TrxR inhibitor, but also used as a TrxR probe. Such theranostic strategies may have great potential for the novel anticancer drug development and cancer treatment.

4. Materials and methods

4.1. Chemistry

All chemicals (reagent grade) used were purchased from Sinopharm Chemical Reagent Co., Ltd. (China). Reaction progress was monitored using analytical thin layer chromatography (TLC) on precoated silica gel GF254 (Qingdao Haiyang Chemical Plant, Qingdao, China) plates and the spots were detected under UV light (254 nm). Melting point was measured on an XT-4 micromelting point instrument and uncorrected. IR (KBr-disc) spectra were recorded by Bruker Tensor 27 spectrometer. ^{1}H NMR and ^{13}C NMR spectra were measured on a Bruker ACF-500 spectrometer at 25 °C and referenced to TMS. Chemical shifts were reported in ppm (δ) using the residual solvent line as internal standard. Splitting patterns were designed as s, singlet; d, doublet; t, triplet; m, multiplet. Mass spectra were obtained on a MS Agilent 1100 Series LC/MSD Trap mass spectrometer (ESI-MS) and a Mariner ESI-TOF spectrometer (HRESI-MS), respectively. Column chromatography was performed on silica gel (90–150 μm; Qingdao Marine Chemical Inc).

Synthesis of 7-(diethylamino)-2H-chromen-2-one (2). A solution of 4-(diethylamino)-2-hydroxybenzaldehyde (**1**, 4.0 g, 446 mmol) and diethyl malonate (9.9 mL, 446 mmol) in ethanol (40 mL) was added piperidine (1 mL). The mixture was reflux for 12 h. After the reaction completed, the solvent was evaporated to obtain the crude ethyl 7-(diethylamino)-2-oxo-2H-chromene-3-carboxylate (**2**). The crude compound **2** was dissolved in hydrochloric acid (20 mL) and glacial acetic acid (20 mL) and refluxed for 18 h. The mixture was cooled to room temperature, poured into ice water (150 mL) and adjusted to pH 5.0 by 1.0 M sodium hydroxide solution. The precipitate was filtered to obtain the pure 7-(diethylamino)-2H-chromen-2-one (**2**). ^{1}H NMR (500 MHz, $CDCl_3$) δ 7.52 (d, J = 9.3 Hz, 1H), 7.23 (d, J = 8.8 Hz, 1H), 6.60 – 6.53 (m, 1H), 6.49 (d, J = 1.8 Hz, 1H), 6.02 (d, J = 9.3 Hz, 1H), 3.40 (q,

J = 7.1 Hz, 4H), 1.20 (t, J = 7.1 Hz, 6H).

Synthesis of 7-(diethylamino)-2-oxo-2H-chromene-3-carbaldehyde (3). 4 mL of dry DMF was added dropwise to 0.4 mL of $POCl_3$ at 20–50 ˚C. The mixture was stirred for 45 min at 50 ˚C under N_2 atmosphere. A suspension of 0.65 g of 7-dimethylamino coumarine in 3 mL of dry DMF is then added, the mixture was warmed to 60 ˚C for 2 h and poured out onto ice water, and the whole was stirred for 2 h. The crystalline precipitate was filtered off, thoroughly washed with water and dried *in vacuo* at 50 ˚C, which afforded an orange solid compound **4** yield 72%.^{1}H NMR (500 MHz, $CDCl_3$) δ 10.09 (s, 1H), 8.22 (s, 1H), 7.39 (d, J = 9.0 Hz, 1H), 6.63 (dd, J = 9.0, 2.3 Hz, 1H), 6.47 (d, J = 2.0 Hz, 1H), 3.46 (q, J = 7.1 Hz, 4H), 1.24 (t, J = 7.1 Hz, 6H).

Synthesis of (E)-7-(diethylamino)-3-(3-oxo-3-phenylprop-1-en-1-yl)-2H-chromen-2-ones. A solution of compound **3** (0.43 mmol) in *N*-butyl alcohol(5 mL) was added to piperidine(0.1 mL), glacial acetic acid (0.1 mL) and different substituted acetophenones (0.43 mmol) and refluxed for 10 h. After the reaction completed determined by TLC, the mixture was concentrated *in vacuo*. The residue was dissolved in dichloromethane and purified by column chromatography eluting with petroleum ether -dichloromethane to afford the products **Xn-1-Xn-14.**

(E)-7-(diethylamino)-3-(3-(3,4-dimethoxyphenyl)-3-oxoprop-1-en-1-yl)-2H-chromen-2-one (**Xn-1**), red solid; m.p. 181–191 ˚C; IR (KBr) v 3456.6, 1713.4, 1629.4, 1575.3, 1520.1, 1420.5, 1276.1, 1200.1, 1163.6, cm-1; ^{1}H NMR (500 MHz, DMSO) δ 8.47 (s, 1H), 8.03 (d, J = 15.4 Hz, 1H), 7.75 (d, J = 8.3 Hz, 1H), 7.64 (d, J = 15.4 Hz, 1H), 7.54 (s, 1H), 7.49 (d, J = 8.9 Hz, 1H), 7.12 (d, J = 8.4 Hz, 1H), 6.79 (d, J = 8.8 Hz, 1H), 6.60 (s, 1H), 3.86 (d, J = 10.7 Hz, 5H), 3.53 – 3.44 (m, 3H), 1.15 (t, J = 6.8 Hz, 6H). ^{13}C NMR (126 MHz, DMSO) δ 160.59 (s), 156.90 (s), 153.60 (s), 149.39 (s), 145.51 (s), 138.84 (s), 131.32 (s), 131.07 (s), 123.36 (s), 121.36 (s), 113.94 (s), 111.46 (s), 111.04 (s), 110.40 (s), 108.84 (s), 96.79 (s), 56.29 (s), 56.06 (s), 44.81 (s), 12.87 (s). HRMS (ESI) m/z 408.1803 $[M + H]^+$ (calcd for 408.1805 $C_{24}H_{26}NO_5$).

(E)-7-(diethylamino)-3-(3-(3-hydroxy-4-methoxyphenyl)-3-oxoprop-1-en-1-yl)-2H-chromen-2-one (Xn-2), red solid; m.p. 98–100 ˚C; IR (KBr) v 3516.5, 2976.7, 1722.9, 1625.7, 1569.5, 1512.6, 1426.9, 1417.4, 1354.8, 1315.1, 1282.6, 1192.3, 1131.4, 1031.6, 1002.8 cm-1; ^{1}H NMR (500 MHz, DMSO) δ 10.04 (s, 1H), 8.46 (s, 1H), 8.02 (d, J = 15.4 Hz, 1H), 7.68 – 7.58 (m, 2H), 7.55 (d, J = 1.8 Hz, 1H), 7.49 (d, J = 9.0 Hz, 1H), 6.93 (d, J = 8.2 Hz, 1H), 6.79 (dd, J = 9.0, 2.3 Hz, 1H), 6.59 (d, J = 2.2 Hz, 1H), 3.86 (s, 3H), 3.48 (q, J = 7.0 Hz, 4H), 1.14 (t, J = 7.0 Hz, 6H). ^{13}C NMR (126 MHz, DMSO) δ 151.76 (d, J = 6.4 Hz), 130.48 (s), 109.84 (s), 96.25 (s), 55.64 (s), 44.27 (s), 40.02 (s), 39.52 (s), 39.35 (s), 39.19 (s), 39.02 (s), 12.34 (s). HRMS (ESI) m/z 394.1647 $[M + H]^+$ (calcd for 394.1649 $C_{23}H_{24}NO_5$).

(E)-7-(diethylamino)-3-(3-(3-methoxyphenyl)-3-oxoprop-1-en-1-yl)-2H-chromen-2-one (Xn-3), red solid; m.p. 121–122 ˚C; IR (KBr) v 3454.7, 1722.7, 1629.7, 1568.3, 1512.1, 1417.9, 1283.1, 1193.2, 1003.4 cm-1; ^{1}H NMR (500 MHz, DMSO) δ 8.49 (s, 1H), 7.98 (d, J = 15.5 Hz, 1H), 7.65 (dd, J = 15.0, 11.7 Hz, 2H), 7.50 (t, J = 8.6 Hz, 3H), 7.23 (dd, J = 8.0, 2.5 Hz, 1H), 6.79 (dd, J = 9.0, 2.3 Hz, 1H), 6.60 (d, J = 2.2 Hz, 1H), 3.84 (s, 3H), 3.52 – 3.42 (m, 4H), 1.14 (t, J = 7.0 Hz, 6H). ^{13}C NMR (126 MHz, DMSO) δ 145.43 (s), 139.39 (d, J = 3.7 Hz), 130.65 (s), 129.96 (s), 120.89 (s), 120.60 (s), 118.79 (s), 109.93 (s), 96.25 (s), 55.32 (s), 44.30 (s), 40.22 – 39.61 (m), 39.52 (s), 39.35 (s), 39.19 (s), 39.02 (s), 12.33 (s). HRMS (ESI) m/z 378.1701 $[M + H]^+$ (calcd for 378.1700 $C_{23}H_{24}NO_4$).

(E)-7-(diethylamino)-3-(3-oxo-3-(p-tolyl)prop-1-en-1-yl)-2H-chromen-2-one (Xn-4), red solid; m.p. 144–146 ˚C; IR (KBr) v 3456.6, 2971.9, 1704.7, 1627.4, 1573.8, 1449.3, 1417.8, 1331.5, 1313.6, 1281.6, 1199.7, 1176.9, 1135.0, 1010.6 cm-1; ^{1}H NMR (500 MHz, DMSO) δ 8.48 (s, 1H), 8.02 (d, J = 15.5 Hz, 1H), 7.95 (d, J = 8.2 Hz, 2H), 7.65 (d, J = 15.4 Hz, 1H), 7.50 (d, J = 9.0 Hz, 1H), 7.38 (d, J = 8.0 Hz, 2H), 6.80 (dd, J = 9.0, 2.4 Hz, 1H), 6.61 (d, J = 2.3 Hz, 1H), 3.48 (q, J = 7.0 Hz, 4H), 2.40 (s, 3H), 1.15 (t, J = 7.0 Hz, 6H). ^{13}C NMR (126 MHz, DMSO) δ 188.41 (s), 159.98 (s), 156.41 (s), 151.88 (s), 145.37 (s), 143.28 (s), 138.98 (s), 135.36 (s), 130.59 (s), 129.36 (s), 128.24 (s), 44.29 (s), 12.33 (s). HRMS (ESI) m/z 362.1749 $[M + H]^+$ (calcd for 362.1751 $C_{23}H_{24}NO_3$).

(E)-7-(diethylamino)-3-(3-oxo-3-(o-tolyl)prop-1-en-1-yl)-2H-chromen-2-one (Xn-5), red solid; m.p. 112–113 ˚C; IR (KBr) v 3855.5, 3483.6, 1716.1, 1619.5, 1577.9, 1510.2, 1419.9, 1355.9, 1320.8, 1273.8, 1193.6, 1134.1, 1011.2 cm-1; ^{1}H NMR (500 MHz, DMSO) δ 8.39 (s, 1H), 7.51 (t, J = 3.5 Hz, 1H), 7.47 (d, J = 8.3 Hz, 2H), 7.43 (dd, J = 10.7, 4.2 Hz, 1H), 7.37 – 7.30 (m, 3H), 6.78 (dd, J = 9.0, 2.3 Hz, 1H), 6.58 (d, J = 2.2 Hz, 1H), 3.47 (q, J = 7.0 Hz, 4H), 2.35 (s, 3H), 1.14 (t, J = 7.0 Hz, 6H). ^{13}C NMR (126 MHz, DMSO) δ 195.19 (s), 159.75 (s), 156.44 (s), 151.97 (s), 145.68 (s), 140.44 (s), 139.19 (s), 135.95 (s), 131.06 (s), 130.70 (s), 130.31 (s), 127.75 (s), 125.66 (s), 125.43 (s), 112.76 (s), 109.90 (s), 108.30 (s), 96.18 (s), 44.28 (s), 19.76 (s), 12.31 (s). HRMS (ESI) m/z 362.1750 $[M + H]^+$ (calcd for 362.1751 $C_{23}H_{24}NO_3$).

(E)-7-(diethylamino)-3-(3-oxo-3-(m-tolyl)prop-1-en-1-yl)-2H-chromen-2-one (Xn-6), red solid; m.p. 155–156 ˚C; IR (KBr) v 3455.8, 1723.7, 1629.5, 1564.8, 1511.0, 1446.3, 1418.9, 1329.6, 1281.7, 1179.5, 1136.9, 1004.1 cm-1; ^{1}H NMR (500 MHz, DMSO) δ 8.48 (s, 1H), 8.00 (d, J = 15.5 Hz, 1H), 7.85 – 7.81 (m, 2H), 7.66 (d, J = 15.4 Hz, 1H), 7.53 – 7.44 (m, 3H), 6.80 (dd, J = 9.0, 2.4 Hz, 1H), 6.60 (d, J = 2.2 Hz, 1H), 3.48 (q, J = 7.0 Hz, 4H), 2.42 (s, 3H), 1.15 (t, J = 7.0 Hz, 6H). ^{13}C NMR (126 MHz, DMSO) δ 189.07 (s), 159.98 (s), 156.44 (s), 151.92 (s), 145.43 (s), 139.23 (s), 138.17 (s), 137.98 (s), 133.49 (s), 130.63 (s), 128.67 (s), 128.45 (s), 125.37 (s), 121.00 (s), 113.21 (s), 109.92 (s), 108.33 (s), 96.26 (s), 44.30 (s), 20.91 (s), 12.33 (s). HRMS (ESI) m/z 362.1752 $[M + H]^+$ (calcd for 362.1751 $C_{23}H_{24}NO_3$).

(E)-7-(diethylamino)-3-(3-(4-fluorophenyl)-3-oxoprop-1-en-1-yl)-2H-chromen-2-one (Xn-7), red solid; m.p. 94–95 ˚C; IR (KBr) v 3457.4, 1723.4, 1627.0, 1513.6, 1416.8, 1355.4, 1287.9, 1198.0, 1134.6, 1010.1 cm-1; ^{1}H NMR (500 MHz, DMSO) δ 8.39 (d, J = 8.8 Hz, 1H), 7.77 – 7.61 (m, 3H), 7.50 (dd, J = 15.8, 12.4 Hz, 2H), 7.41 – 7.32 (m, 2H), 6.78 (dd, J = 9.0, 2.2 Hz, 1H), 6.58 (d, J = 2.0 Hz, 1H), 3.53 – 3.43 (m, 4H), 1.13 (dd, J = 9.1, 5.1 Hz, 6H). ^{13}C NMR (126 MHz, DMSO) δ 188.71 (s), 187.05 (s), 159.60 (s), 159.02 (s), 156.48 (s), 152.09 (s), 146.53 (s), 140.45 (s), 133.90 (d, J = 8.8 Hz), 130.78 (s), 130.26 (d, J = 2.8 Hz), 127.16 (d, J = 13.6 Hz), 124.72 (dd, J = 20.2, 4.1 Hz), 116.61 (s), 116.43 (s), 112.69 (s), 109.93 (s), 108.35 (s), 96.17 (s), 44.31 (s), 12.32 (s). HRMS (ESI) m/z 366.1498 $[M + H]^+$ (calcd for 366.1500 $C_{22}H_{21}FNO_3$).

(E)-3-(3-(4-bromophenyl)-3-oxoprop-1-en-1-yl)-7-(diethylamino)-2H-chromen-2-one (Xn-8), red solid; m.p. 209–211 ˚C; IR (KBr) v 3455.4, 1707.8, 1620.6, 1574.4, 1510.9, 1412.2, 1314.1, 1280.0, 1196.6, 135.2, 1067.6, 1004.3 cm-1; ^{1}H NMR (500 MHz, DMSO) δ 8.49 (s, 1H), 8.02 – 7.95 (m, 3H), 7.79 (d, J = 8.5 Hz, 2H), 7.67 (d, J = 15.4 Hz, 1H), 7.49 (d, J = 9.0 Hz, 1H), 6.80 (dd, J = 9.0, 2.4 Hz, 1H), 6.61 (d, J = 2.2 Hz, 1H), 3.49 (d, J = 7.1 Hz, 4H), 1.15 (t, J = 7.0 Hz, 6H). ^{13}C NMR (126 MHz, DMSO) δ 159.93 (s), 156.51 (s), 152.05 (s), 145.84 (s), 139.97 (s), 131.88 (s), 130.72 (s), 130.12 (s), 120.40 (s), 113.04 (s), 110.01 (s), 108.35 (s), 96.27 (s), 44.33 (s), 12.34 (s). HRMS (ESI) m/z 426.0696 $[M + H]^+$ (calcd for 426.0699 $C_{22}H_{21}BrNO_3$).

(E)-3-(3-(4-butylphenyl)-3-oxoprop-1-en-1-yl)-7-(diethylamino)-2H-chromen-2-one (Xn-9), red solid; m.p. 70–71 ˚C; IR (KBr) v 3452.2, 2927.6, 1705.9, 1625.9, 1574.8, 1514.2, 1448.8, 1416.5, 1331.9, 1314.1, 1281.2, 1201.0, 1175.1, 1133.1, 1008.1 cm-1; ^{1}H NMR (500 MHz, DMSO) δ 8.47 (s, 1H), 8.02 (d, J = 15.5 Hz, 1H), 7.96 (d, J = 8.2 Hz, 2H), 7.64 (d, J = 15.4 Hz, 1H), 7.49 (d, J = 9.0 Hz, 1H), 7.39 (d, J = 8.2 Hz, 2H), 6.79 (dd, J = 9.0, 2.4 Hz, 1H), 6.60 (d, J = 2.3 Hz, 1H), 3.48 (q, J = 7.0 Hz, 4H), 2.69 – 2.62 (m, 2H), 1.61 – 1.55 (m, 2H), 1.32 (dd, J = 14.9, 7.5 Hz, 2H), 1.14 (t, J = 7.0 Hz, 6H), 0.90 (t, J = 7.4 Hz, 3H). ^{13}C NMR (126 MHz, DMSO) δ 188.45 (s), 159.98 (s), 156.41 (s), 151.88 (s), 147.97 (s), 145.40 (s), 138.98 (s), 135.62 (s), 130.60 (s), 128.70 (s), 128.27 (s), 120.95 (s), 113.26 (s),

109.90 (s), 108.33 (s), 96.24 (s), 44.29 (s), 34.77 (s), 32.71 (s), 21.72 (s), 13.70 (s), 12.34 (s). HRMS (ESI) *m/z* 404.2219 $[M + H]^+$ (calcd for 404.222 $C_{22}H_{21}BrNO_3$).

(E)-7-(diethylamino)-3-(3-(4-ethoxyphenyl)-3-oxoprop-1-en-1-yl)-2H-chromen-2-one (Xn-10), red solid; m.p. 128–130 °C; IR (KBr) v 3455.4, 1704.7, 1631.2, 1597.8, 1513.7, 1420.0, 1336.9, 1312.1, 1265.2, 1202.2, 1167.3, 997.5 cm-1; ^{1}H NMR (500 MHz, DMSO) δ 8.46 (s, 1H), 8.03 (dd, J = 8.8, 5.8 Hz, 3H), 7.62 (d, J = 15.4 Hz, 1H), 7.49 (d, J = 9.0 Hz, 1H), 7.08 (d, J = 8.9 Hz, 2H), 6.79 (dd, J = 9.0, 2.4 Hz, 1H), 6.59 (d, J = 2.2 Hz, 1H), 4.14 (q, J = 7.0 Hz, 2H), 3.48 (q, J = 7.0 Hz, 4H), 1.36 (t, J = 7.0 Hz, 3H), 1.14 (t, J = 7.0 Hz, 6H). ^{13}C NMR (126 MHz, DMSO) δ 188.45 (s), 156.90 (s), 131.04 (s), 121.44 (s), 114.97 (s), 110.42 (s), 108.85 (s), 96.78 (s), 64.07 (s), 44.81 (s), 14.99 (s), 12.87 (s). HRMS (ESI) *m/z* 392.1855 $[M + H]^+$ (calcd for 392.1856 $C_{24}H_{26}NO_4$).

(E)-3-(3-(2,4-dichlorophenyl)-3-oxoprop-1-en-1-yl)-7-(diethylamino)-2H-chromen-2-one (Xn-11), red solid; m.p. 208–210 °C; IR (KBr) v 3456.3, 1712.9, 1622.1, 1568.9, 1514.6, 1419.2, 1360.4, 1325.7, 1034.8 cm-1; ^{1}H NMR (500 MHz, DMSO) δ 8.54 (s, 1H), 8.21 (d, J = 1.9 Hz, 1H), 8.04 – 7.92 (m, 2H), 7.86 (d, J = 8.4 Hz, 1H), 7.71 (d, J = 15.4 Hz, 1H), 7.50 (d, J = 9.0 Hz, 1H), 6.81 (dd, J = 9.0, 2.3 Hz, 1H), 6.61 (d, J = 2.2 Hz, 1H), 3.49 (q, J = 7.0 Hz, 4H), 1.15 (s, 6H). ^{13}C NMR (126 MHz, DMSO) δ 187.28, 157.14 (s), 146.13 (s), 131.72 (s), 131.32 (s), 130.41 (s), 128.71 (s), 120.39 (s), 110.58 (s), 108.87 (s), 96.83 (s), 44.87 (s), 12.87 (s). HRMS (ESI) *m/z* 416.0813 $[M + H]^+$ (calcd for 416.0815 $C_{22}H_{20}Cl_2NO_3$).

(E)-7-(diethylamino)-3-(3-(3-hydroxyphenyl)-3-oxoprop-1-en-1-yl)-2H-chromen-2-one (Xn-12), red solid; m.p. 152–153 °C; IR (KBr) v 3455.5, 1721.5, 1624.5, 1555.2, 1446.7, 1417.2, 1329.6, 1286.2, 1188.9, 1132.4, 1032.1, 1004.3 cm-1; ^{1}H NMR (500 MHz, DMSO) δ 9.82 (s, 1H), 8.43 (s, 1H), 7.97 (t, J = 12.4 Hz, 1H), 7.62 (d, J = 15.2 Hz, 1H), 7.47 (d, J = 8.5 Hz, 2H), 7.38 (dd, J = 16.7, 8.9 Hz, 2H), 7.04 (d, J = 7.5 Hz, 1H), 6.77 (d, J = 8.1 Hz, 1H), 6.58 (s, 1H), 3.52 – 3.42 (m, 4H), 1.13 (t, J = 6.8 Hz, 6H). ^{13}C NMR (126 MHz, DMSO) δ 189.37 (s), 160.43 (s), 158.22 (s), 156.92 (s), 152.43 (s), 146.32 (s), 139.83 (d, J = 4.0 Hz), 131.14 (s), 130.37 (s), 121.54 (s), 120.52 (s), 119.51 (s), 114.91 (s), 113.71 (s), 110.44 (s), 108.87 (s), 96.75 (s), 44.82 (s), 12.86 (s). HRMS (ESI) *m/z* 364.1540 $[M + H]^+$ (calcd for 364.1543 $C_{22}H_{22}NO_4$).

(E)-7-(diethylamino)-3-(3-(4-nitrophenyl)-3-oxoprop-1-en-1-yl)-2H-chromen-2-one (Xn-13), red solid; m.p. 174–176 °C; IR (KBr) v 3451.6, 2967.9, 2924.4, 1687.1, 1614.6, 1579.1, 1512.2, 1448.0, 1415.9, 1352.9, 1327.4, 1279.7, 1192.5, 1132.4, 1012.7 cm-1; ^{1}H NMR (500 MHz, DMSO) δ 8.51 (s, 1H), 8.39 (d, J = 8.8 Hz, 2H), 8.23 (d, J = 8.8 Hz, 2H), 8.01 (d, J = 15.4 Hz, 1H), 7.71 (d, J = 15.4 Hz, 1H), 7.51 (d, J = 9.0 Hz, 1H), 6.81 (dd, J = 9.0, 2.4 Hz, 1H), 6.62 (d, J = 2.2 Hz, 1H), 3.50 (d, J = 7.1 Hz, 4H), 1.15 (t, J = 7.0 Hz, 6H). ^{13}C NMR (126 MHz, DMSO) δ 188.66 (s), 160.37 (s), 157.16 (s), 152.76 (s), 150.17 (s), 147.01 (s), 143.38 (s), 141.68 (s), 131.40 (s), 129.98 (s), 124.48 (s), 120.93 (s), 110.62 (s), 108.93 (s), 96.80 (s), 44.89 (s), 12.87 (s). HRMS (ESI) *m/z* 393.1442 $[M + H]^+$ (calcd for 393.1445 $C_{22}H_{21}N_2O_5$).

(E)-3-(3-(4-aminophenyl)-3-oxoprop-1-en-1-yl)-7-(diethylamino)-2H-chromen-2-one (Xn-14), red solid; m.p. 152–153 °C; IR (KBr) v 3455.4, 2972.8, 1717.7, 1620.3, 1583.5, 1511.8, 1411.5, 1344.2, 1323.8, 1280.5, 1195.1, 1133.8, 1080.7, 977.8 cm-1; ^{1}H NMR (500 MHz, DMSO) δ 8.73 – 8.68 (m, 1H), 8.53 (s, 1H), 8.51 – 8.43 (m, 2H), 8.05 (d, J = 15.4 Hz, 1H), 7.88 (t, J = 8.0 Hz, 1H), 7.76 (d, J = 15.4 Hz, 1H), 7.51 (d, J = 9.0 Hz, 1H), 6.81 (dd, J = 9.0, 2.4 Hz, 1H), 6.62 (d, J = 2.2 Hz, 1H), 3.50 (d, J = 7.1 Hz, 4H), 1.15 (t, J = 7.0 Hz, 6H). ^{13}C NMR (126 MHz, DMSO) δ 187.72 (s), 160.44 (s), 157.15 (s), 152.71 (s), 148.67 (s), 146.75 (s), 141.52 (s), 139.63 (s), 134.75 (s), 131.38 (s), 131.20 (s), 127.58 (s), 122.95 (s), 120.39 (s), 113.35 (s), 110.60 (s), 108.91 (s), 96.81 (s), 44.88 (s), 12.88 (s). HRMS (ESI) *m/z* 364.1546 $[M + H]^+$ (calcd for 364.1543 $C_{22}H_{22}N_2O_3$).

Maintenance of Cell Lines Culture and Cell Viability Assays. All cell lines were purchased from Cell Bank of Shanghai Institute of Biochemistry and Cell Biology, Chinese Academy of Sciences (Shanghai, China). Human colon carcinoma cells HCT116 and human normal liver cells L02 were maintained in DMEM medium. All cells were supplemented with 12% fetal bovine serum containing 50 μg/mL penicillin and 50 μg/mL streptomycin. Cells were grown to 80% confluency in a tissue culture flask at 37 °C in a humidified atmosphere containing 5% CO_2, and then were trypsinized with 1 × Trypsin-Versene and splitted.

Cells (HCT116) were seeded in 96-well plates at a density of 4000–6000 cells per well. The cells were incubated at 37 °C overnight (16 h) in a humidified 5% CO_2 incubator. After medium removal, different concentrations of test compounds were added in triplicate to the plates in 200 μL fresh mediums, the plates were incubated at 37 °C for 72 h.The percentage of DMSO in the medium not exceeded 0.1%. 3-(4,5-Dimethylthiazolyl)-2,5-diphenyltetrazoliumbro-mide (MTT) was added to evaluate cell viability. The absorbance was read by an ELISA reader (SpectraMax Plus384, Molecular Devices, Sunnyvale,CA) at a test wavelength of 570 nm and a reference wavelength of 630 nm. Cell viability was calculated by the following formula:

$$\% \text{ Cell viability} = (At/As) \times 100\%$$

At and As denoted the absorbance of the test substances and solvent control, respectively.

Western Blot Analysis. HCT116 cells were incubated with various concentrations of **Xn-2** for 24 h. Harvesting after trypsinisation, cells were treated with 1 × RIPA lysis buffer (50 mM Tris–HCl, pH 7.4, 150 mM NaCl, 0.25% deoxycholic acid, 1% NP-40, 1 mM EDTA and protease inhibitors) (Amresco, Solon, USA) to extract thetotal proteins. An aliquot of proteins from the total cell lysates (30 to 60 μg/lane) was separated by sodium dodecyl sulfate (10%) polyacrylamide gelelectrophoresis (SDS–PAGE, BioRad Laboratories, Hercules, CA), wet-transferred to NC membrane (BioRad Laboratories, Hercules, CA) and blotted with primary antibodies specific for TrxR, Cleaved PARP, Bcl-2, Bax and GAPDH. Bound immuno-complexes were detected using ChemiDOC™ XRS + system (BioRad Laboratories, Hercules, CA).

Detection of ROS. HCT116 cells were seeded at a density of 1.5×10^4 per well of 96-well plates or 3×10^5 per well of 6-well plates. The cells were treated with various concentrations of **Xn-2** for 24 h. DCFH-DA was dissolved in Serum-free medium and diluted to a final concentration of 10 μM. After treatment with **Xn-2**, the growth media was replaced with serum-free medium containing the probe. After incubation for 30 min at 37 °C, cells were washed with serum-free medium twice, digested by trypsin and resuspended in the pre-warmed PBS buffer. The samples were then subjected an ImageXpress Micro Confocal analysis.

Detection of apoptosis. HCT116 cells were seeded at a density of 1.5×10^4 per well of 96-well plates. The cells were treated with various concentrations of **Xn-2** for 24 h. Hoeschst 33,342 was dissolved in Serum-free medium and diluted to a final concentration of 5 μg/mL. After incubation for 30 min at 37 °C, cells were washed with serum-free medium twice, digested by trypsin and resuspended in the pre-warmed PBS buffer. The samples were then subjected to an ImageXpress Micro Confocal analysis.

Trans-well Invasive Assays. HCT116 Cells treatment with or without **Xn-2** were seeded at 2×10^4 cells per well (0.2 mL) and allowed to grow for 24 h. After being fixed in 4% of paraformaldehyde for 10 min. Crystal violet solution (Sigma, St. Louis, MO,USA) was used to stain the colonies for 4 h. The migration of cells was visualized at x200 magnification using a Microscope.

Colony survival assay. HCT116 cells were cultured 800–1000 per well in 6-well plate with regular growth medium. Cells were treated by vehicle and **Xn-2** at different concentrations on the following day for 24 h. Cells were allowed to grow for 10–14 d until the colonies were visible. Crystal violet solution (Sigma, St. Louis, MO, USA) was used to stain the colonies for 4 h and colonies were scored manually as described previously.

Molecular Docking Studies. The crystal structure of TrxR1 in complex with the inverse agonist (PDB code: 3EAN.pdb) was downloaded from Protein Data Bank (http://www.pdb.org). All the ligand and protein preparations were performed in Maestro (version 9.4, Schrdinger, LLC, New York, NY, 2013) implemented in the Schrdinger program. The proteins were prepared using the Protein Preparation Wizard within Maestro 9.4 (Schrdinger, LLC). Hydrogens were added, bond orders were assigned, and missing side chains for some residues were added using Prime. The added hydrogens were subjected to energy minimization until the root-mean-square deviation (RMSD) relative to the starting geometry reached 0.3 Å. For Glide docking, the grid was defined using a 20 Å box centered on the ligand, and the important water molecules around ligand were kept. All parameters were kept as default. The designed molecules were docked using Glide SP mode, and the predicted binding modes of all the compounds were ranked according to their glidescores.

Declaration of Competing Interest

The authors declare no competing financial interest.

Acknowledgements

This research work was supported by National Natural Science Foundation of China (Grant No. 81671682) and Hospital fund of the First Affiliated Hospital of Zhengzhou University. We thanks for the help of docking studies by PhD. wu xishan in Guangdong Provincial Key Laboratory of Biocomputing, Joint School of Life Sciences, Guangzhou Institutes of Biomedicine and Health, Chinese Academy of Sciences for the help of Molecular Docking Studies.

Author Contributions

All authors have given approval to the final version of the manuscript.

Appendix A. Supplementary material

Supplementary data to this article can be found online at https://doi.org/10.1016/j.bioorg.2019.103530.

References

[1] A. Brown, Q. Shi, T.W. Moore, Y. Yoon, A. Prussia, C. Maddox, D.C. Liotta, H. Shim, J.P. Snyder, J. Med. Chem. 56 (2013) 3456.
[2] B. Zhang, J. Zhang, S. Peng, R. Liu, X. Li, Y. Hou, X. Han, J. Fang, Expert Opin. Ther. Pat. 27 (2017) 547.
[3] S. Wu, Q. Cao, X. Wang, K. Cheng, Z. Cheng, Chem. Commun. 50 (2014) 8919.
[4] H.L. Ng, S. Chen, E.H. Chew, W.K. Chui, Eur. J. Med. Chem. 115 (2016) 63.
[5] L. Xie, Z. Luo, Z. Zhao, T. Chen, J. Med. Chem. 60 (2017) 202.
[6] D. Hu, Y. Liu, Y.T. Lai, K.C. Tong, Y.M. Fung, C.N. Lok, C.M. Che, Angewandte Chemie 55 (2016) 1387.
[7] S.R. Jean, D.V. Tulumello, C. Riganti, S.U. Liyanage, A.D. Schimmer, S.O. Kelley, ACS Chem. Biol. 2015 (2007) 10.
[8] B. Liang, W. Shao, C. Zhu, G. Wen, X. Yue, R. Wang, J. Quan, J. Du, X. Bu, ACS Chem. Biol. 11 (2016) 425.
[9] C.-P.T. Rui-Rong Ye, Liang-Nian Jia, Zong-Wan Mao, Dalton Trans. 33 (2016) 13042.
[10] M. Bhatia, K.L. McGrath, G. Di Trapani, P. Charoentong, F. Shah, M.M. King, F.M. Clarke, K.F. Tonissen, Redox Biol. 8 (2016) 68.
[11] B. Zhang, D. Duan, C. Ge, J. Yao, Y. Liu, X. Li, J. Fang, J. Med. Chem. 58 (2015) 1795.
[12] H.L. Ng, X. Ma, E.H. Chew, W.K. Chui, J. Med. Chem. 60 (2017) 1734.
[13] S. Banerjee, A.R. Chakravarty, Acc. Chem. Res. 48 (2015) 2075.
[14] W.Q. Chen, P.Z. Zou, Z.W. Zhao, Q.Y. Weng, X. Chen, S.L. Ying, Q. Ye, Z. Wang, J.S. Ji, G. Liang, Oncotarget 7 (2016) 16593.
[15] M. Jovanović, D. Zhukovsky, A. Podolski-Renić, I. Domračeva, R. Žalubovskis, M. Senćanski, S. Glišić, V. Sharoyko, T. Tennikova, D. Dar'in, M. Pešić, M. Krasavin, Eur. J. Med. Chem. (2019) 111580.
[16] D. Subramaniam, R. May, S.M. Sureban, K.B. Lee, R. George, P. Kuppusamy, R.P. Ramanujam, K. Hideg, B.K. Dieckgraefe, C.W. Houchen, S. Anant, Cancer Res. 2008 (1962) 68.
[17] S. Xu, S. Luo, H. Yao, H. Cai, X. Miao, F. Wu, D.H. Yang, X. Wu, W. Xie, H. Yao, Z.S. Chen, J. Xu, J. Med. Chem. 59 (2016) 5022.
[18] S. Li, H. Wang, L. Hong, W. Liu, F. Huang, J. Wang, P. Wang, X. Zhang, J. Zhou, Cancer Biol. Ther. 16 (2015) 176.
[19] W. Li, S.M. Saud, M.R. Young, N.H. Colburn, B. Hua, Mol. Cell. Biochem. 406 (2015) 63.
[20] A. Bisi, C. Cappadone, A. Rampa, G. Farruggia, A. Sargenti, F. Belluti, R.M. Di Martino, E. Malucelli, A. Meluzzi, S. Iotti, S. Gobbi, Eur. J. Med. Chem. 127 (2017) 577.
[21] M.L. Manca, I. Castangia, M. Zaru, A. Nacher, D. Valenti, X. Fernandez-Busquets, A.M. Fadda, M. Manconi, Biomaterials 71 (2015) 100.
[22] W. Zhang, W. Yu, G. Cai, J. Zhu, C. Zhang, S. Li, J. Guo, G. Yin, C. Chen, L. Kong, Cell Death Dis. 9 (2018) 1098.
[23] W.Y. Kim, H. Shi, H.S. Jung, D. Cho, P. Verwilst, J.Y. Lee, J.S. Kim, Chem. Commun. 52 (2016) 8675.
[24] A.R. Sarkar, C.H. Heo, L. Xu, H.W. Lee, H.Y. Si, J.W. Byun, H.M. Kim, Chemistry Science 7 (2016) 766.
[25] K.M. Zhang, W. Dou, P.X. Li, R. Shen, J.X. Ru, W. Liu, Y.M. Cui, C.Y. Chen, W.S. Liu, D.C. Bai, Biosens. Bioelectron. 64 (2015) 542.
[26] X. Zhang, Q. Ba, Z. Gu, D. Guo, Y. Zhou, Y. Xu, H. Wang, D. Ye, H. Liu, Chemistry 21 (2015) 17415.
[27] W. Zhang, F. Liu, C. Zhang, J.G. Luo, J. Luo, W. Yu, L. Kong, Anal. Chem. 89 (2017) 12319.
[28] W. Zhang, Y. Wang, J. Dong, Y. Zhang, J. Zhu, J. Gao, Dyes Pigm. 171 (2019) 107753.
[29] T. Liu, J. Zhang, X. Han, J. Xu, Y. Wu, J. Fang, Free Radical Biol. Med. 135 (2019) 216–226.
[30] R. Liu, D. Shi, J. Zhang, X. Han, X. Yao, J. Fang, Molecular Pharaceutics 15 (2018) 3285–3296.
[31] J. Zhang, J. Yao, S. Peng, X. Li, J. Fang, BBA-Mole. Basis Disease 1 (2017) 129–138.
[32] J. Zhang, Y. Li, D. Duan, J. Yao, K. Gao, J. Fang, Biochem. Pharmacol. 102 (2016) 34–44.
[33] X. Li, B. Zhang, C. Yan, J. Li, S. Wang, X. Wei, X. Jiang, P. Zhou, J. Fang, Nat. Commun. 10 (2019) 2745.
[34] L. Zhang, D. Duan, Y. Liu, C. Ge, X. Cui, J. Sun, J. Fang, J. Am. Chem. Soc. 136 (2014) 226–233.